Innovative: International Multi-disciplinary Journal of Applied Technology
(ISSN 2995-486X) VOLUME 02 ISSUE 07, 2024

A Comprehensive Investigation on Electronic Structure and Optical Properties of the Hfsse Janus Monolayer

Ghufran Falah Ibrahim, Manar Salman Toman
University of Babylon, College of Education for pure sciences, Department of physics, Iraq

Abstract:

First-principles simulations according to the linearized enhanced full-potential planewave (FP-LAPW) approach They were used to thoroughly examine the optical, thermoelectric, and electronic structure characteristics of the HfSSe Janus monolayer. The HfSSe A Janus monolayer exhibits dynamic stability, according to the results. The two-dimensional (2D) material under consideration has electronic characteristics that suggest it is an indirect gap semiconductor. The Wu-Cohen technique under the approximation of the generalised gradient (GGA-WC) yielded a band gap of 0.620 eV.

A narrower band gap of 0.553 eV results from the inclusion of spin-orbit connection (SOC) as calculated, which disrupts the valence and transmission bands' degeneracy. Furthermore. According to the results of its optical characteristics, the 2D monolayer under study would be a good choice to practice for nano-optoelectronic apparatus if it has a high absorption coefficient of around 103/cm and a wider consumption band that can be extended from the apparent to the ultraviolet.

In essence, the study employed a theory founded by Boltzmann one of the semi-classical paradigms, titled; transport theory to calculate the thermoelectric characteristics, such as power factor, electronic thermal conductivity, electrical conductivity and Seebeck coefficient. The findings suggest that electron doping might be advantageous for the HfSSe Janus monolayer's thermoelectric performance because of its higher power factor values when in comparison with hole doping.

Keywords: *First principles, Comprehensive investigation, calculations, HfSSe Janus monolayer, Electronic structure, Optical items.*

1. Introduction

The field of electronics and optoelectronics has drawn huge attention in recent time from various scholars, especially, on bi-dimensional (2D) conversion metal di-chalcogenides (TMDCs) because of its unusual density of states, band gap tunability, atomically thick layer, and mechanical strength[1]. With an appropriate band gap beyond 2D Graphene, they can be extremely promising materials for electrical applications, according to several experimental and theoretical investigations [2], optoelectronic[3], thermoelectric[4], gas detection [5], dividing of water [6] as well as piezoelectric uses [7]. These TMDCs are materials being coated with extremely weak layered Van-der-Waal contact, where a solitary layer consisting of single transition metal deposit is sandwiched by binary chalcogen atom coats. Their typical formula is MXY, where M=Mo, W, Hf, Zr, Pt, etc. and X,Y=S, Se, as well as Te. Just lately, Ang-Yu Lu and co[8] created a novel form of TMDCs known as Janus single-layer MoSSe, which has smashed in-plane through symmetry inversion and out-of-plane assumed mirror symmetry. This was achieved by completely substituting Se atoms for S atoms in the top layer of monolayer MoS2. Numerous investigations on the electrical, gas sensing, optical, photocatalytic, mechanical, thermoelectric, in consonance with mechanical characteristics of Janus TMDCs had been conducted. These enquiries were motivated in one way or the other by Janus mono-layer's Mosse examination.[9][10].

2. Computational Methods

Electrical and optical properties of monolayer items; HFXY (XY= S, Se) are investigated by DFT methods, that was executed by the CASTEP software Added to exploiting The PBE, exchange-correlation energy functional, and ultrasoft pseudopotentials [11], [12]. The Brillouin zones are tested with 16×16×1 Monkhorst-Pack grid with k mesh. The computations were carried out by using 30×30×1 figure Monkhorst pack to compute the presumed optical characteristics, use k-mesh, and for massive state computing, this sum will be applied 24×24×1. The level of k-point is essential when the optical band materials are being illustrated, especially, with the presupposed component of the dielectric function. For plane wave basis, all computations are performed at 520 eV, which is the kinetic energy cut-off. Each and every atom in these Janus structures is fully relaxed, and the convergence needed for the complete energy as well as the force for the total energy and the force reacting on the atoms are, correspondingly, 10^{-6} eV and 0.01 eV/Å.

In the Z-direction, a 30 Å vacuum gap was employed to inhibit the interplay between the adjacent monolayers. Nonetheless, another functional perturbation theory was used to examine the optical features within the energy point of 0 to 25 eV. These features include the total energy cost function L(ω), the reflectivity R(ω), the refraction index n(ω), the presumptive (Im(ε(ω)) and actual (Re(ε(ω)) portions of the dielectric role ε(ω), and the absorption coefficient α(ω). ω has shown indicates the occurrence of incident photons.

2. Electronic Structure of Monolayer

Figure (1) shows the structure of HFSSe monolayer that are used in the present study, one can see from the figure that each simulated system consists of a 4× 4×1 supercell. These materials are arranged in hexagonal structures composed of layers joined together by vdW connections. Each layer has furnace monoatomic blades arranged in HFSSe [13] has a symmetry of D3h. HFSSe contain a hexagonal clear structure with a related space composition P3m1 [14]. These items can be considered appropriate in order to dissociate water from optoelectronic devices, electro-optical selection, and non-linear optics, which including photovoltaics, phototransistors, field-effect transistors, photodiodes, and photoresistors [15]. It has been reported that the HFSSe monolayer exhibits thermal stability and possesses an irregular energy vacuum spanning a broad optical spectrum [16]–[18]. Gallium telluride has a moderate but direct bandgap in huge form, measuring around 1.67 eV [19], [20]

that promotes the formation of these two elements; excitons and photon which may later be absorbed completely. Since the majority of the Sun's radioactivity falls within the observed range, photovoltaics requires a certain energy band gap: between 1.5 and 2.5 eV. Nonetheless, the depth or the total number of layers of the HFSSe material has a considerable impact on its band gap. Long carrier lifetimes and extremely strong photoresponsivity exceeding 10^4 A/W are displayed by the HFSSe monolayer [21], Remarkable photoluminescence [22], [23], photodetectors with a brief reaction time of approximately 6 ms and at least, a robust excitonic production and absorption [24]. As a result, HFSSe monolayers are seen as a potential material for applications including radiation detectors (γ and X-ray), solar energy, thermoelectric devices, photocatalysis, and phototransistors [14], [25]–[28]. Even if The term photoresponsivity of HFSSe multidimensional simulations is greater than that of grapheme photodetectors (0.13 A/W) and MoS2 monolayer (880 A/W), despite the extremely low observed mobility of charge carriers[21], [29], [30]. It is noteworthy that several research groups have expressed interest in the characteristics of vdW heterostructures based on HFSSe; nonetheless, the optical properties of the HFSSe monolayers remain mostly unexplored and require additional investigation. This work has led to the employment of In this work, we use first-principles scheming according to DFT computations to completely assess the electrical and optical characteristics of the HFSSe monolayers.

Table 1: Bond length Å and the band angle of Hfsse monolayer.

Bond length Å		Bond angle (degree)	
Hf – Se	2.693	Hf – Se – Hf	87.240
Hf – S	2.584	Hf – S – Hf	91.961
Hf – Hf	3.716	Hf – Se – S	43.643
Se – S	3.743	Hf – S – Se	46.006
S – S	3.716	S – Hf – Se	90.35
Se - Se	3.716		

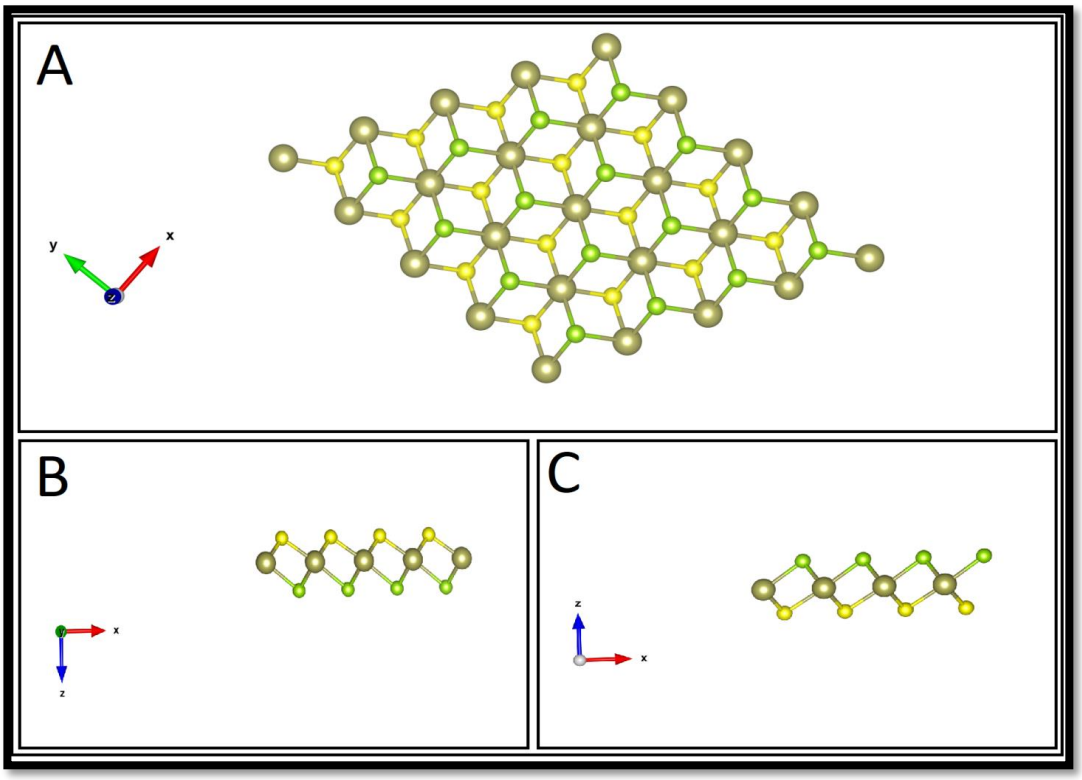

Fig. (1): presentation of top-view, b and c side-view of HFSSe elements monolayer.

1.2. Band Structure

The electrical-band set-up of a solid is (energy levels) the type of energy series whereby an electron found in a solid nature are identified as bands or allowable bands. Similarly, the energy of those ranges not having an electron within the solid called band gap or forbidden bands. Because the energy bands have finite widths, band gaps are basically residual energy ranges that are not covered by any band. The widths of the bands vary, based on how much the atomic orbitals from which they originate overlap. It's interesting to see from Fig. (2) shows the HFSSe monolayer's band structures indicate an irregular band gap, primarily because the actual CBM is situated at the almost M point, while the VBM is positioned amid the Γ and K spots. Using calculations from basic principles, the HFSSe monolayer's indirect band gap property has been shown [31], [32]. The PBE functional calculates that the HFSSe monolayer's indirect gap (ΓK–M) is 0.620 eV, whereas the direct gap (Γ–Γ) is 0 eV.

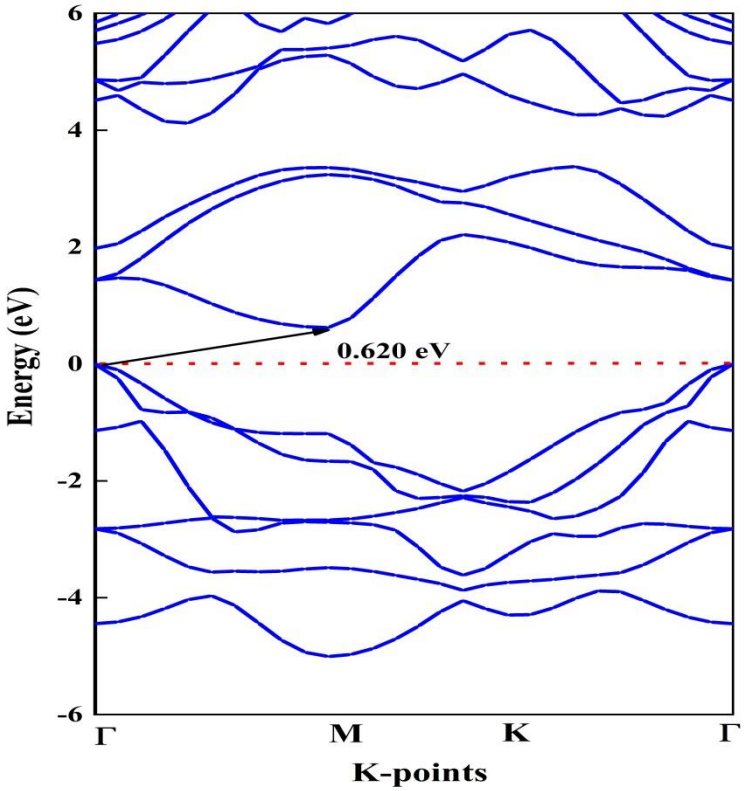

Fig. (2): Band structure of HFSSe monolayer.

2.2 Density of States

Specify winch Plotting the rotational components in the density of states is necessary. In a spin-polarized system, distinct density of states for those specific electrons containing spin-up and spin-down can be enhanced. The graph-total density of states is derived by summing across all energy bands. Their difference yields the approximate spin mass of states, and their addition yields the overall density of states. One relevant idea is the volume of state, which makes it possible to employ integration with regard to electron energy rather than integration over the Brillouin zone. Furthermore, the density of state is frequently employed for a rapid electron structure investigation. Additionally useful in understanding the alterations in electronic structure brought about by external pressure can be identified with density of state (DOS) analysis.

Analysis of partial density of states (PDOS) For high-energy narrated in the transmission band, the formalism is invalid; the partial density of states representation often decays to zero at a potential energy of 20 eV above the Fermi level. This has to do with the fact that it is difficult to expand the

basically free electron state in terms of a finite number of atomic-like basis functions accurately. In a partial density of states plot, these related terms valance band as well as the bottommost portion in the conduction band are significant. The s, p, d, and f can be used to regulate the angular momenta to be included in the partial density of states. An effective semi-qualitative technique for examining electronic structure is the partial density of states. By rotating these contributions in accordance with the angular momentum of the states, PDOS further validates these findings. It's frequently used to determine where the major peaks of the s, p, or d character in the DOS are located.

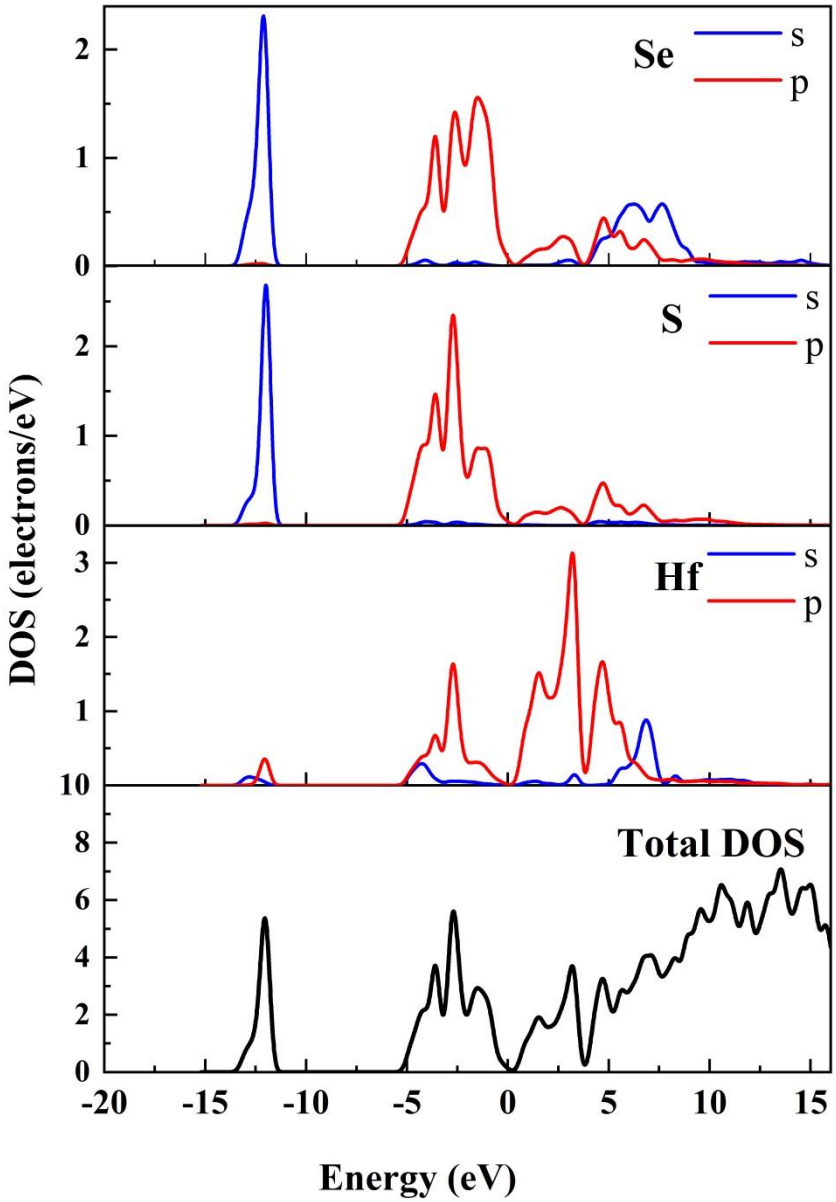

Fig (3): Density of state of HFSSe monolayer.

The figure 3 highlights the electrical entire quantity of states (DOS) for the monolayers of Se, S, and HF. Examining the overall DOS reveals a variety of van Hove singularities throughout the whole energy spectrum, that is attached to a monolayer material's two-dimensional structure.

Likewise, the pseudo-atomic calculation for Se 4s2 4p4 gathered in 19 reiterations to the whole energy of -256.4822ev, and also the atomic sum for S 3s2 3p4 obtained in 20 confirmed iterations

realized to a complete energy of -273.8555ev. The quasi-atomic addition of HF 5d2 6s2 addressed in 20 iterations to a whole energy of -401.5064ev.

3. Optical Properties

It goes without saying that basic research and contemporary applications heavily rely on the optical characteristics of materials. For example, the accuracy of the refraction index limits the use of safe optical techniques to infer the composition of an alloy or the epitaxial layers. The deduction of the dielectric constants and the accuracy of identification of refraction index with dielectric constants and combined structure are indicated. As a result, we have calculated the optical parameters, including the dielectric function, loss function, conductivity, refraction index, reflectivity, and absorption coefficient. Calculations have been made for these optical characteristics up to 25 eV in energy.

3.1 Dielectric Function

The elaborate dielectric function can be used to evaluate the optical characteristics $\varepsilon(\omega) = \varepsilon_1(\omega) + \iota\varepsilon_2(\omega)$. The fictitious component of the dielectric function corresponds to a material's primary optical characteristics; for HFSSe monolayer, the actual and supposed components of the dielectric role have a single main peak that occurs at precisely 3.48 and 3.25 eV. The transitions of direct electrons often from the valency band point to the conduction band may primarily be responsible for the peaks. It is found that the area of lower energies is where the largest peaks in the actual and assumed components of the dielectric constant seek to migrate, which points out that every photon from the event is reflected in this area. The so-called redshift is this. It is noteworthy that these monolayers' imaginary part's main peaks are similar to their real part counterpart's main peaks, as seen in Fig. (4). It is commonly known that the imaginary component of the dielectric function significantly affects the medium's absorption. There is an indication that a lot of peaks which compound the imagery section may result to modification in band. As a result, a unified peak around the tentative portion indicates the presence of a single valence band to conduction band inter-band transition. John and Merlin [33] report that there is correspondence between the actual stenene segment and HFSSe mono-layer’s main peak.

The calculated rigid dielectric serves at zero photon energy limits are 2.65 monolayer, in that order. The HFSSe monolayer's static dielectric constant is lower than the 4.7 value discovered previously for layered HFSSe utilizing Heyd-Scuseria-Ernzerhof (HSE06)[34]. Conversely, in the parallel polarization direction, the fixed dielectric, and very constant values of HFSSe mono-layer are less than those of well-known 2D materials and equivalent to that of graphene [33]. Although the dielectric constant is a crucial component in calculating capacitance, a high static dielectric constant might be advantageous for producing capacitors.

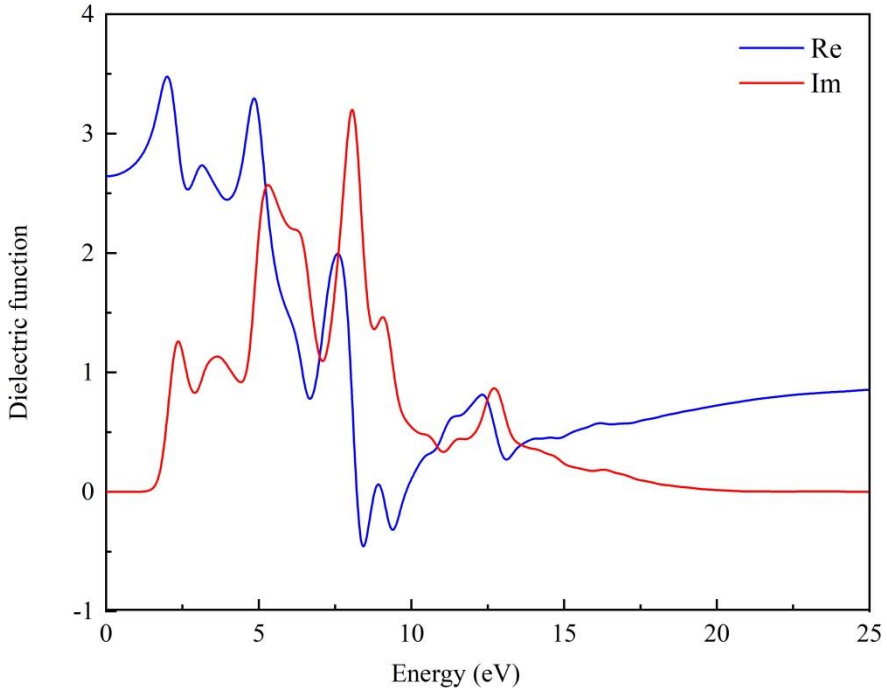

Fig (4): Dielectric function of HFSSe monolayer.

3.2 Absorption Coefficient

If the light's frequency is in resonance with the medium's atoms' transition frequencies, absorption takes place via propagation. The beam in this instance will diminish as it progresses. Since only light that hasn't been absorbed will be conveyed, there is an evident connection between the absorption and medium transmission. A lot of optical materials get their color via absorption. For instance, ruby absorbs green and blue light but not red, which is why it appears red..

The absorbent coefficient, or ct, of an optical material measure how much light it can absorb. The percentage of power consumed in a single unit length of the medium is the definition of this. A certain amount of energy is absorbed by materials as light passes through them. Equation (1) illustrates how to calculate the absorption coefficient, α, which indicates how much radiation energy a material has absorbed.

$\alpha=2\omega k/c=4\pi k/\lambda$ (1)

where k serves as the emission coefficient, λ takes the radiation wavelength, ω represents the cyclic frequency, and c occupies the position of the speediness of light in a vacuum.

The inverse optical response valence from the bands to the lowest conducting bands is represented by the absorption coefficient (α) [35]. The electric dielectric function may be used to directly infer the absorption [35],[26]. When estimating a material's optical characteristics for usage in optoelectronic devices, the optical absorption spectrum is crucial. The percentage of light intensity attenuation that occurs when a light wave travels a unit distance in a specific material is known as the absorption coefficient. With regard to the absorption coefficients shown in Fig. (5), the primary peaks are located at 8.321 eV. This indicates that there is observable absorption of monolayer at the UV region. Additionally, this work shows that the HFSSe monolayer's absorption peaks are strikingly comparable to those of one-layer GeP, SiP, and GeP, and to have feature primary absorption peaks in the UV spectrum[36], This shows HFSSe single layers, particularly in the UV region, have more promise for use in photoelectric devices. It is clear that there is a near-interconnection between absorption and the generated part of the dielectric role. It was found out that the imaginary angle that the HFSSe monolayer absorption power takes effect at 1.81eV, placing it inside the visible light spectrum. This absorption edge is in proximity to the UV–vis absorption

maxima of bigger aromatic molecules and silicene functionalized with phenyl[37]. The UV absorption edge is crucial for photocatalytic activity in practical applications

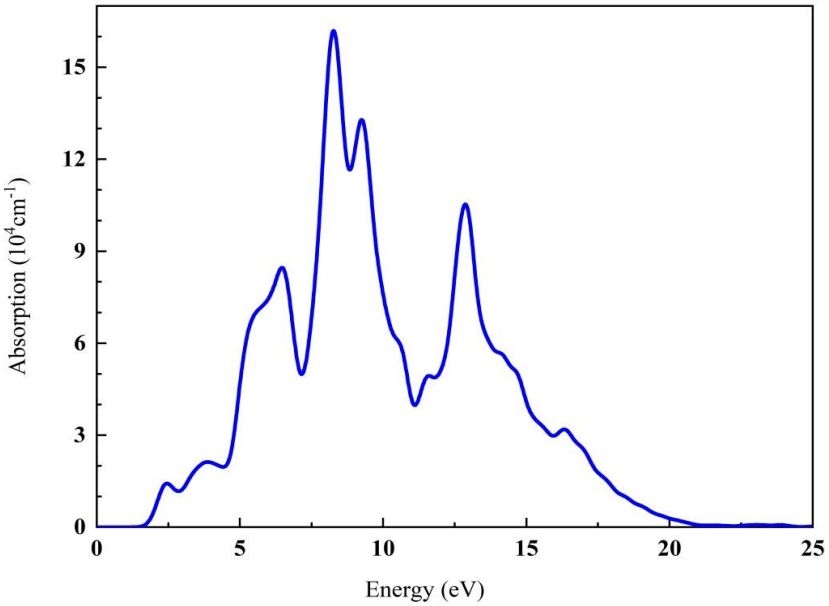

Fig. (5): Absorption of HFSSe monolayer

3.3 Conductivity

This section presents an instance of the total optical conduction as a role of energy across the limit of 0–25 eV is presented in Fig. (6). For HFSSe monolayer, conductivity begins at 2.18 eV of energy. However, for the HFSSe monolayer, the curves move to the highest optical conduction at peak 7.91eV. This conductivity is greater than the optical one of germanene, silicene, and graphene honeycomb crystals.

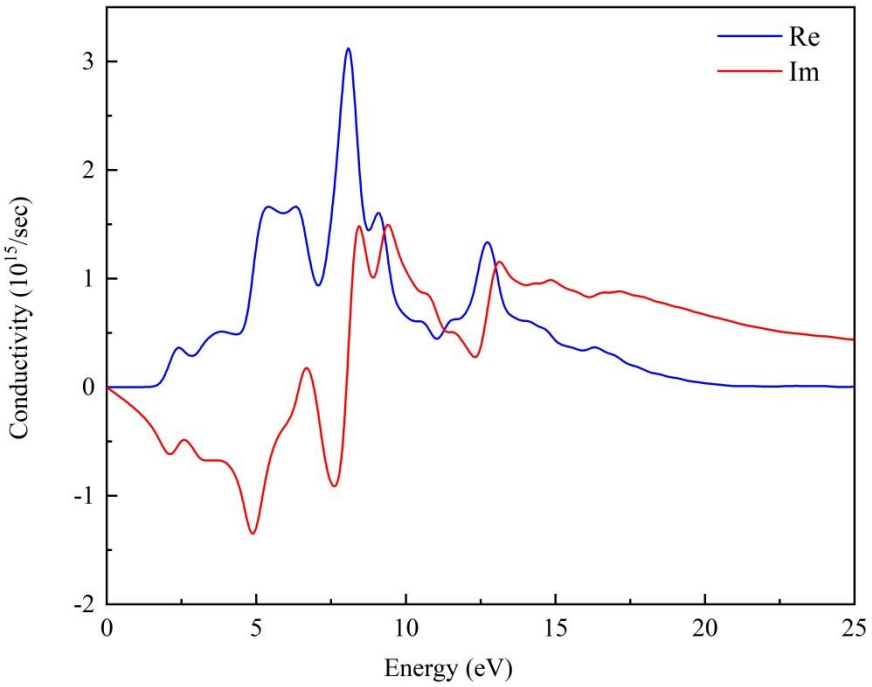

Fig (6): Conductivity of HFSSe monolayer.

3.4 Loss Function

The loss function, a crucial statistic that illustrates the uncontrollably dispersing high-speed electrons across a material and describes the associated plasma frequency, is another significant function of optical features that this work has clarified. Together with their associated resonance, the energy loss points define the mixed plasma reoccurrence, Below the plasma regularity, the material exhibits dielectric properties, and below it, its metallic character is revealed. The energy loss peak for the HFSSe monolayer is located at 11.13 eV, whereas the primary sharp peak is at this same energy. This energy indicates the point at which the monolayer's metallic to dielectric properties change; as seen in Fig. (7), the energy loss reduces when photon energy increases beyond these levels. The ultraviolet (UV) area is where the monolayer's highest energy loss functions occur. As a result, these monolayers may effectively absorb the twin radiation namely, low-medium on one hand and low-ultraviolet radiation on the other. Therefore, the present monolayers can be applied in the solar cell. As usual, the energy forfeiture peaks depict the plasma occurrence. To be more specific, any given material acts as a metallic material above a certain frequency and as a dielectric at lesser values.

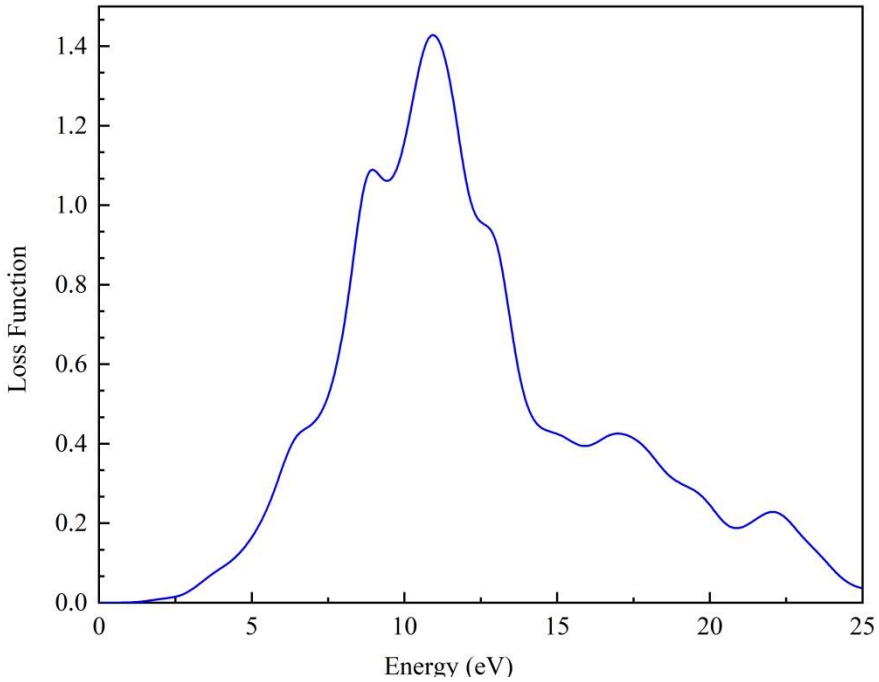

Fig. (7): Loss functions of HFSSe monolayer.

3.5 Reflectivity

The calculated reflectivity as a stand of energy is shown in Fig. (8), where it is discovered that the static reflectivity is 5.82 eV for monolayers. This value is about zero value frequency, while the domination of free carriers is achieved. Above this point, the curve shows an increase in reflectance as photon energy increases.

The middle UV region has the highest reflectivity values, which are 28%. This suggests that the maximum reflectivity value is not always more than 28%.

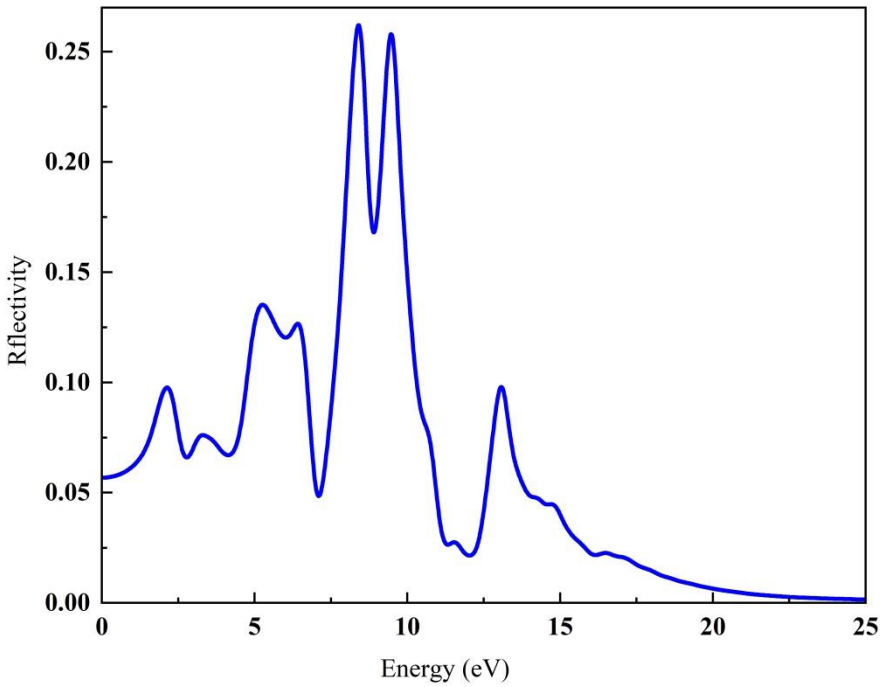

Fig. (8): Reflectivity of HFSSe monolayer.

3.6 Refractive Index (n)

A clear medium's beam propagation may be explained by the refractive index, or n. The ratio of light's velocity in free space to its velocity in the medium is known as this.

The light beam's frequency affects the refractive index. Dispersion is the term for this phenomenon. The proportion of light velocity within a velocity to phase velocity of light in a substance is known as the real refractive index. As so, it shows the phase velocity at which light passes through a substance. Refractive index rises with incident radiation frequency in a normal dispersion. Real refractive index deviates from normal dispersion and suffers a reduction at strong absorptions of radiation energy by a material; this is anomalous dispersion with increase The optoelectronic characteristics of materials are significantly influenced by the refraction index. At zero photon energy, the real component static refractive indices of HFSSe monolayer are equal to 1.644. The greatest refractive index (real part) value for HFSSe monolayer is 1.910, occurring at about 3.383 eV. The refractive index steadily drops after this point. These monolayers may serve other functions within the inner layer coating between the substrate as well as UV- UV-engaging layer because of their high refractive indices. These monolayers have an anisotropic refractive index. Conversely, in the ultraviolet region, the HFSSe monolayer's extinction coefficient (imaginary component) rapidly decreases as photon energy increases and reaches a constant value at 24 eV.

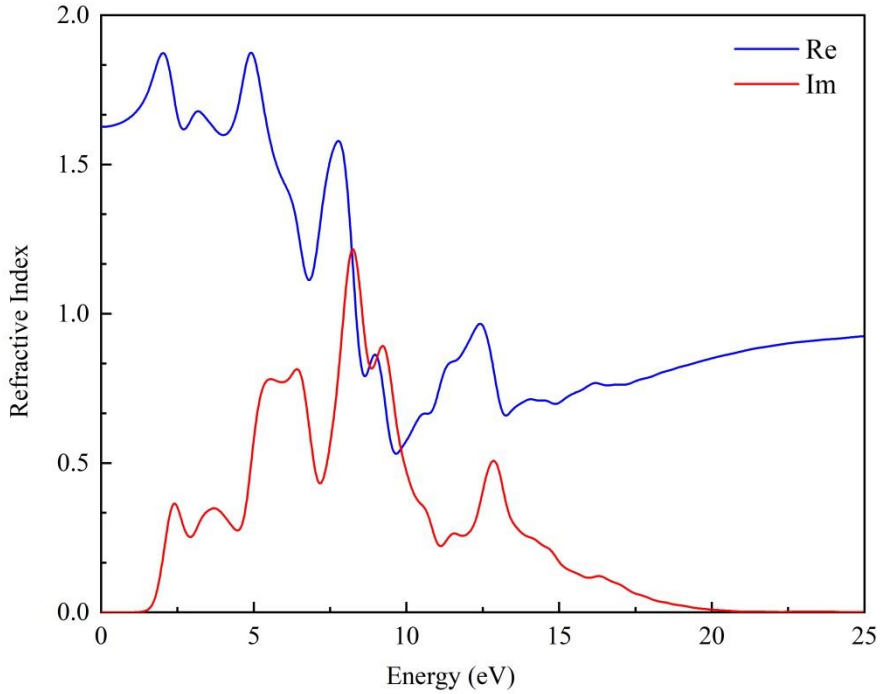

Fig. (9): Refractive index of HFSSe monolayer**.**

References

1. Q. H. Wang, K. Kalantar-Zadeh, A. Kis, J. N. Coleman, and M. S. Strano, "Electronics and optoelectronics of two-dimensional transition metal dichalcogenides," *Nat. Nanotechnol.*, vol. 7, no. 11, pp. 699–712, 2012.
2. P. Johari and V. B. Shenoy, "Tuning the electronic properties of semiconducting transition metal dichalcogenides by applying mechanical strains," *ACS Nano*, vol. 6, no. 6, pp. 5449–5456, 2012.
3. K. F. Mak and J. Shan, "Photonics and optoelectronics of 2D semiconductor transition metal dichalcogenides," *Nat. Photonics*, vol. 10, no. 4, pp. 216–226, 2016.
4. D. Qin, P. Yan, G. Ding, X. Ge, H. Song, and G. Gao, "Monolayer PdSe 2: A promising two-dimensional thermoelectric material," *Sci. Rep.*, vol. 8, no. 1, pp. 1–8, 2018.
5. F. K. Perkins, A. L. Friedman, E. Cobas, P. M. Campbell, G. G. Jernigan, and B. T. Jonker, "Chemical vapor sensing with monolayer MoS2," *Nano Lett.*, vol. 13, no. 2, pp. 668–673, 2013.
6. D. Voiry, J. Yang, and M. Chhowalla, "Recent strategies for improving the catalytic activity of 2D TMD nanosheets toward the hydrogen evolution reaction," *Adv. Mater.*, vol. 28, no. 29, pp. 6197–6206, 2016.
7. M. J. Mleczko *et al.*, "HfSe2 and ZrSe2: Two-dimensional semiconductors with native high-κ oxides," *Sci. Adv.*, vol. 3, no. 8, p. e1700481, 2017.
8. Y. Lu *et al.*, "Magnetic modification of GaSe monolayer by absorption of single Fe atom," *RSC Adv.*, vol. 7, no. 8, pp. 4285–4290, 2017, doi: 10.1039/C6RA27309B.
9. Z. Guan, S. Ni, and S. Hu, "Tunable electronic and optical properties of monolayer and multilayer Janus MoSSe as a photocatalyst for solar water splitting: a first-principles study," *J. Phys. Chem. C*, vol. 122, no. 11, pp. 6209–6216, 2018.
10. G.-X. Chen, H.-F. Li, D.-D. Wang, S.-Q. Li, X.-B. Fan, and J.-M. Zhang, "Adsorption of toxic gas molecules on pristine and transition metal doped hexagonal GaN monolayer: A first-principles study," *Vacuum*, vol. 165, pp. 35–45, Jul. 2019, doi:

10.1016/J.VACUUM.2019.04.001.

11. J. Clark Stewart *et al.*, "First principles methods using CASTEP," *Zeitschrift für Kristallographie - Crystalline Materials*, vol. 220. pp. 567–570, 2005, doi: 10.1524/zkri.220.5.567.65075.
12. J. P. Perdew, K. Burke, and M. Ernzerhof, "Generalized Gradient Approximation Made Simple," *Phys. Rev. Lett.*, vol. 77, no. 18, pp. 3865–3868, Oct. 1996, doi: 10.1103/PhysRevLett.77.3865.
13. S. Yang, C. Jiang, and S. Wei, "Gas sensing in 2D materials," *Appl. Phys. Rev.*, vol. 4, no. 2, p. 21304, 2017, doi: 10.1063/1.4983310.
14. H. L. Zhuang and R. G. Hennig, "Single-Layer Group-III Monochalcogenide Photocatalysts for Water Splitting," *Chem. Mater.*, vol. 25, no. 15, pp. 3232–3238, 2013, doi: 10.1021/cm401661x.
15. X. Wang *et al.*, "Enhanced rectification, transport property and photocurrent generation of multilayer ReSe2/MoS2 p–n heterojunctions," *Nano Res.*, vol. 9, no. 2, pp. 507–516, 2016.
16. S. Demirci, N. Avazlı, E. Durgun, and S. Cahangirov, "Structural and electronic properties of monolayer group III monochalcogenides," *Phys. Rev. B*, vol. 95, no. 11, p. 115409, 2017.
17. X. Zhang, S. Wang, G. Wan, Y. Zhang, M. Huang, and L. Yi, "Transient reflectivity measurement of photocarrier dynamics in GaSe thin films," *Appl. Phys. B*, vol. 123, no. 3 LB-Zhang2017, p. 86, 2017, doi: 10.1007/s00340-017-6677-z.
18. O. Del Pozo-Zamudio *et al.*, "Photoluminescence of two-dimensional GaTe and GaSe films," *2D Mater.*, vol. 2, no. 3, p. 035010, Jul. 2015, doi: 10.1088/2053-1583/2/3/035010.
19. K. Çınar, Z. Çaldıran, C. Coşkun, and Ş. Aydoğan, "Electrochemical growth of GaTe onto the p-type Si substrate and the characterization of the Sn/GaTe Schottky diode as a function of temperature," *Thin Solid Films*, vol. 550, pp. 40–45, 2014, doi: https://doi.org/10.1016/j.tsf.2013.10.034.
20. S. Pal and D. N. Bose, "Growth, characterisation and electrical anisotropy in layered chalcogenides GaTe and InTe," *Solid State Commun.*, vol. 97, no. 8, pp. 725–729, 1996, doi: https://doi.org/10.1016/0038-1098(95)00608-7.
21. F. Liu *et al.*, "High-Sensitivity Photodetectors Based on Multilayer GaTe Flakes," *ACS Nano*, vol. 8, no. 1, pp. 752–760, Jan. 2014, doi: 10.1021/nn4054039.
22. I. Caraman, N. Spalatu, I. Evtodiev, D. Untila, L. Leontie, and M. Caraman, "Photoelectric and photoluminescence properties of CdTe-GaTe composite," *Phys. status solidi*, vol. 253, no. 12, pp. 2515–2522, Dec. 2016, doi: 10.1002/pssb.201600485.
23. D. N. Bose and S. Pal, "Photoconductivity, low-temperature conductivity, and magnetoresistance studies on the layered semiconductor GaTe," *Phys. Rev. B*, vol. 63, no. 23, p. 235321, May 2001, doi: 10.1103/PhysRevB.63.235321.
24. A. Zubiaga, J. A. García, F. Plazaola, V. Muñoz-Sanjosé, and C. Martínez-Tomás, "Near band edge recombination mechanisms in GaTe," *Phys. Rev. B*, vol. 68, no. 24, p. 245202, Dec. 2003, doi: 10.1103/PhysRevB.68.245202.
25. S. Huang *et al.*, "In-Plane Optical Anisotropy of Layered Gallium Telluride," *ACS Nano*, vol. 10, no. 9, pp. 8964–8972, Sep. 2016, doi: 10.1021/acsnano.6b05002.
26. J. Susoma *et al.*, "Second and third harmonic generation in few-layer gallium telluride characterized by multiphoton microscopy," *Appl. Phys. Lett.*, vol. 108, no. 7, p. 073103, Feb. 2016, doi: 10.1063/1.4941998.

27. K. Xu *et al.*, “Short channel field-effect transistors from ultrathin GaTe nanosheets,” *Appl. Phys. Lett.*, vol. 107, no. 15, p. 153507, Aug. 2015, doi: 10.1063/1.4933346.

28. A. J. Nelson *et al.*, “X-ray photoemission analysis of chemically treated GaTe semiconductor surfaces for radiation detector applications,” *J. Appl. Phys.*, vol. 106, no. 2, p. 23717, Aug. 2009, doi: 10.1063/1.3176478.

29. O. Lopez-Sanchez, D. Lembke, M. Kayci, A. Radenovic, and A. Kis, “Ultrasensitive photodetectors based on monolayer MoS2,” *Nat. Nanotechnol.*, vol. 8, p. 497, 2013, doi: 10.1038/nnano.2013.100 https://www.nature.com/articles/nnano.2013.100#supplementary-information.

30. X. Wang, Z. Cheng, K. Xu, H. K. Tsang, and J.-B. Xu, “High-responsivity graphene/silicon-heterostructure waveguide photodetectors,” *Nat. Photonics*, vol. 7, no. 11, pp. 888–891, Nov. 2013, doi: 10.1038/nphoton.2013.241.

31. Y. Ma, Y. Dai, M. Guo, L. Yu, and B. Huang, “Tunable electronic and dielectric behavior of GaS and GaSe monolayers,” *Phys. Chem. Chem. Phys.*, vol. 15, no. 19, pp. 7098–7105, 2013.

32. Y. Li, H. Chen, L. Huang, and J. Li, “Ab Initio Study of the Dielectric and Electronic Properties of Multilayer GaS Films,” *J. Phys. Chem. Lett.*, vol. 6, no. 6, pp. 1059–1064, 2015, doi: 10.1021/acs.jpclett.5b00139.

33. R. John and B. Merlin, “Optical properties of graphene, silicene, germanene, and stanene from IR to far UV – A first principles study,” *J. Phys. Chem. Solids*, vol. 110, pp. 307–315, 2017, doi: https://doi.org/10.1016/j.jpcs.2017.06.026.

34. B. P. Bahuguna, L. K. Saini, R. O. Sharma, and B. Tiwari, “Structural, electronic and optical properties of layered GaSe1−xAsx,” *Comput. Mater. Sci.*, vol. 139, pp. 31–38, Nov. 2017, doi: 10.1016/J.COMMATSCI.2017.07.020.

35. S. Y. Zhou *et al.*, “Substrate-induced bandgap opening in epitaxial graphene,” *Nat. Mater.*, vol. 6, no. 10, pp. 770–775, Oct. 2007, doi: 10.1038/nmat2003.

36. Y. Cheng, R. Meng, C. Tan, X. Chen, and J. Xiao, “Selective gas adsorption and I–V response of monolayer boron phosphide introduced by dopants: A first-principle study,” *Appl. Surf. Sci.*, vol. 427, pp. 176–188, Jan. 2018, doi: 10.1016/J.APSUSC.2017.08.187.

37. H. Ye *et al.*, “SnSe monolayer: A promising candidate of SO2 sensor with high adsorption quantity,” *Appl. Surf. Sci.*, vol. 484, pp. 33–38, Aug. 2019, doi: 10.1016/J.APSUSC.2019.03.346.